Frontiers in Heat and Mass Transfer

Tech Science Press

DOI: 10.32604/fhmt.2024.053688

ARTICLE

Study of the Influence of the Distance between Smoke Outlets and Fire Source on Smoke Flow Characteristics in Tunnel Fires

Liang Yi, Zhiqiang Lei, Zhisheng Xu, Yaolong Yin and Houlin Ying*

School of Civil Engineering, Central South University, Changsha, 410083, China

*Corresponding Author: Houlin Ying. Email: evelynlin@csu.edu.cn

Received: 07 May 2024 Accepted: 17 June 2024 Published: 30 August 2024

ABSTRACT

This paper explores the smoke flow characteristics in tunnel fires, giving a particular emphasis on the effects of different distances between the smoke outlets and the fire source. It examines the smoke behavior under different conditions, including variations in heat release rates, exhaust volumetric flow rates, spacing between smoke outlets, and the longitudinal fire source positions. Results indicate that altering the fire source positions and the smoke outlets in the tunnel leads to variations in the properties of smoke flow both the fire source upstream and downstream; the distance between fire source and smoke outlet increases gradually, airflow rate decreases initially and eventually reaches a stable state. Similarly, smoke mass flow rate exhibits an increasing trend that eventually reaches a stable state. Moreover, the heat exchange between the tunnel walls and hot smoke increases as the smoke outlet moves further away from the fire source. This interaction leads to a reduction in the heat exhaust coefficient and a decrease in the distance the smoke spreads. This study investigates the impact of altering the relative longitudinal fire source positions and smoke outlet on smoke flow characteristics by numerical simulation. A theoretical analytical method is used to give a predictive model for the heat exhaust coefficient and the smoke spreading distance. This research can support the theory and technical process of tunnel smoke exhaust prevention and control.

KEYWORDS

Tunnel fire; numerical simulation; centralized smoke exhaust; heat exhaust coefficient; smoke spreading distance

1 Introduction

In the last twenty years, the number of tunnels had significant increase. Tunnels have become an important means of alleviating traffic pressure and optimizing traffic layout, providing convenient transportation options for people's travel. The rise in the quantity of tunnels raises the probability of fire incidents occurring [1,2]. Examples include the appearance of a fire in Mont Blanc Tunnel [3] and another fire in Yanhou Tunnel [4] culminated in numerous fatalities and substantial financial damages. The safety of individuals' lives is endangered by the smoke from fires, and about 85% of victims die from toxic smoke [5]. Mechanical smoke extraction is frequently employed to manage smoke and ensure the safety of individuals within the tunnel, while also creating a suitable environment for rescuers to conduct operations. There are three main methods of mechanical exhaust extraction

in tunnels: longitudinal smoke extraction, centralized smoke extraction from the top, and lateral smoke extraction. Numerous researchers have extensively studied centralized smoke extraction, with a primary emphasis on enhancing smoke exhaust efficiency and minimizing the distance smoke spreads.

The mechanical smoke extraction system performance is a vital measure to evaluate the smoke extraction system's efficacy. Vauquelin [6] examined the smoke extraction system's effectiveness and suggested two crucial parameters that would evaluate the smoke extraction system's capability by means of the utilization of the cold smoke study methodology. However, this cold smoke experimental approach differs from the actual burning situation. The reason for this is that heat transfer was not considered. Plug-holing causes cold air to flow into the smoke outlets, diminishing the volume of hot smoke that is released. This ends up resulting in higher energy usage. Li et al. [7] applied a critical Froude number to approximate the plug-holing probability by performing computational simulations with varying exhaust velocities and heat release rates. Furthermore, a parameter for identifying the initiation of plug-holing was obtained. Jiang et al. [8] performed investigations to propose an evaluation principle for non-plug-holing, the transitional stage, and the appearance of plug-holing by experiments. According to Zhao et al. [9], the exhaust volumetric flow rate at which plug-holing occurs increases when the heat release rate (HRR) and aspect ratio expand. This was shown in small-scale experiments where HRRs and smoke outlet settings were varied. Furthermore, when the smoke outlet area grows, the exhaust volumetric flow rate at which plug-holing happens also increases. Yi et al. [10] utilized a series of experiments and investigated the system's efficiency in terms of heat removal. Moreover, the heat exhaust coefficient increases when the outlets are located in closer proximity to the fire source. Yan et al. [11] conducted a series of numerical simulations to investigate the smoke control efficiency in a large cross-section tunnel equipped with a two-point central smoke extraction system. The results indicated that a higher smoke exhaust rate increases the smoke control efficiency and the longer smoke outlet perpendicular to the longitudinal axis of the tunnel can control smoke better than the shorter one. Liu et al. [12] analyzed the synergistic effect of smoke outlet layout and smoke extraction rate on the performance of the central smoke extraction system. Their results showed that increasing the smoke extraction rate and smoke outlet width can improve the ventilation system efficiency.

Smoke spreading can impede escape and rescue, and smoke must be removed from the tunnel in a reasonable way. Li et al. [13] made a model that calculates the dimensionless smoke spreading distance, taking into account the effects of longitudinal ventilation. In view of this idea, Chen et al. [14] modified the dimensionless smoke spreading distance model created by Li et al. [13] and developed a computational model to forecast the distance at which smoke spreads in a tunnel with one exhaust outlet positioned above the fire source by applying the fire source heat release rate modifying method. Then, Chen et al. [15] investigated situations in which the exhaust outlet positioned the fire source downstream and subsequently modified the aforementioned model by doing experiments on the same small-scale model. Based on the same theory, Tang et al. [16] performed studies using the identical tunnel model and examined the scenario in which the smoke outlet is positioned before the fire source. Wang et al. [17] established a unified smoke spreading distance prediction model by combining the physical laws of conservation of energy and mass to quantify the smoke spreading distances for these three scenarios. Jiang et al. [18] established an equation that defines the correlation between the distance at which smoke spreads and the rate of induced airflow in a centralized smoke exhaust system with only two smoke outlets, derived from small-scale model experiments. Liu et al. [19] proposed a predictive model for the back-layering length of the smoke downstream of the centralized smoke outlet considering the smoke exhaust efficiency, smoke outlet layout, and the distance between the fire source and smoke outlet by combining the physical laws of conservation of energy and mass.

However, a significant portion of the prior research was carried out under the expectation that the fire source exists in the tunnel's center and that it is equidistant from smoke outlets on both sides, or there is only one smoke outlet. The issue of smoke development could be segmented into four clearly defined stages: the stage of plume ascent, the stage of radial spread, the transition stage, and the one-dimensional horizontal spread stage [20]. If the fire source is equidistant from both exhaust outlets, the smoke should move in a symmetrical manner in both directions. However, if the fire source is not symmetrical from both smoke outlets, the hot smoke created by the combustion of the fire source will not be at an equal distance from the smoke outlets. So there exist disparities in the reduction of velocity, the behavior of air entrainment, and the transmission of heat on the fire source both upstream and downstream [21]. In this study, we focus on the difference in smoke flow characteristics upstream and downstream of the fire. This work aims to examine the variations in smoke flow characteristics resulting from the alteration in the longitudinal fire source location while considering variable HRRs, exhaust volumetric flow rates, and smoke outlet spacing by integrating theoretical analysis with numerical simulation. Based on the discussion of the influence of relative longitudinal fire sources, a predictive model applied heat release rate modifying method for smoke spreading distance was proposed. This study hopes to contribute to the development of both the theoretical framework and technical methods for tunnel smoke emission prevention and control.

2 Numerical Modeling

The continuous advancement of computer technology has empowered Fire Dynamics Simulator (FDS) to handle increasingly complex, sophisticated, and accurate numerical calculations. Numerical simulation has a more significant advantage in adjusting variable conditions and obtaining detailed parameter distributions than experimentation. The FDS has become prevalent in different fire scenarios, like tunnel fire [22,23], compartment fire [24,25], energy storage station fire [26], and its efficacy has been well-proven. In this study, FDS was used for numerical simulation studies.

2.1 Model Construction

As displayed in Fig. 1, the horizontal road tunnel was designed using the FDS, a modeling system that replicates the tunnel environment. The tunnel has measurements of 500 m in length, 5 m in width, and 9 m in height. Two smoke outlets were positioned in the model tunnel ceiling, each measuring 5 by 2 m. The smoke outlet's short side lies parallel to the tunnel's longitudinal axis. The distance from one smoke outlet to another was designated as D_e, which varied from 60 to 100 m at an interval of 20 m. The fire source is positioned along the tunnel's longitudinal axis and is positioned between two smoke outlets. d was defined as the distance between the fire source and a single smoke outlet. More specifically, d_1 is the distance between the fire source and its upstream smoke outlet, and d_2 is the distance between the fire source and its downstream smoke outlet. When the fire source exists at the initial position, d_1 is 5 m. To study the impact of varying lengths from the fire to smoke outlets on smoke characteristics, the fire source was relocated from its initial position to the midpoint of the two smoke outlets in increments of 5 m until d_1 was equal to d_2. In the tunnel equipped with the centralized smoke extraction system, the top smoke duct is connected to external shafts at both ends. The fans in both shafts will switch on at the same time after the occurrence of fire. Thus, the exhaust volumetric flow rates upstream and downstream are the same in the smoke duct, as shown in Fig. 1.

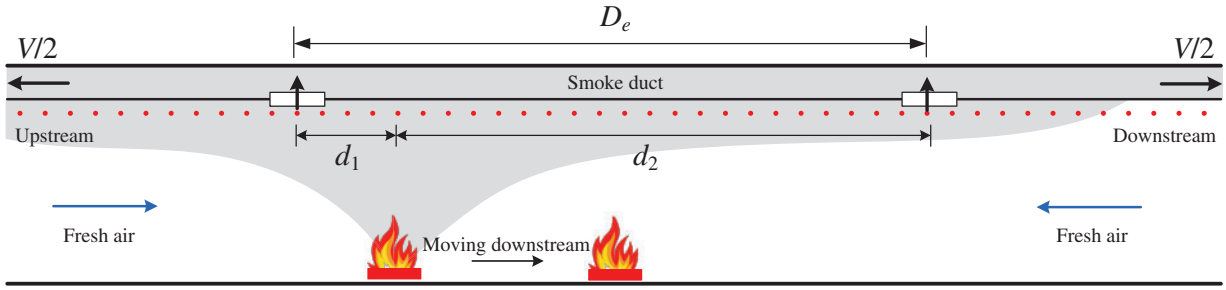

(A) Font view

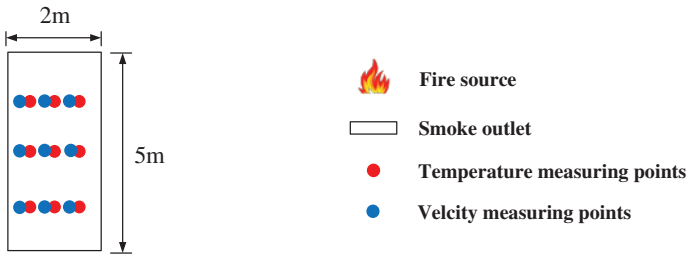

(B) Distribution of measuring points at the smoke outlet

Figure 1: Model tunnel configuration

By dictating a heat release rate per unit area over a 4 m^2 square solid surface which is parallel with the floor, the fire source boundary conditions have been established. The current temperature of the surroundings is 293 K, and the current pressure of the surroundings is 101 kPa. Temperature sensors were strategically set up 0.2 m below the tunnel ceiling centerline, spaced with a spacing of 1 m along the tunnel longitudinal axis. Nine measurement points for temperature and velocity were strategically positioned at the smoke outlet.

2.2 Simulated Conditions

In sum, 147 test cases were established, as detailed in Table 1. Three smoke outlet spacing and 6∼10 longitudinal fire source positions were considered. The heat release rates were set at 3, 5, and 10 MW, to simulate vehicle fire [27]. The exhaust volumetric flow rates were 60, 80, 100, and 120 m^3/s.

Table 1: Summary of test cases

No.	D_e (m)	d_1 (m)	d_2 (m)	$\dot{Q}$ (MW)	V (m^3/s)
T01-03	/	/	/	3,5,10	/
T04-27	60	5,10,15,20,25,30	55,50,45,40,35,30	3	60,80,100,120
T28-51	60	5,10,15,20,25,30	55,50,45,40,35,30	5	60,80,100,120
T52-75	60	5,10,15,20,25,30	55,50,45,40,35,30	10	60,80,100,120
T76-107	80	5,10,15,20,25,30, 35,40	75,70,65,60,55,50, 45,40	5	60,80,100,120
T108-147	100	5,10,15,20,25,30, 35,40,45,50	95,90,85,80,75,70, 65,60,55,50	5	60,80,100,120

2.3 Grid Quality Verification

The size of the grid is a vital factor that directly impacts the precision of the simulation outputs. Optimal grid size has significance for achieving accurate numerical simulation results and ensuring computational efficiency. In numerical simulations, the dimensionless parameter D^*/δ_x was employed to assess the grid quality across various fire scenarios. D^* can be expressed as follows [28]:

$$D^* = \left(\frac{\dot{Q}}{\rho_a c_p T_a \sqrt{g}} \right)^{\frac{5}{2}} \tag{1}$$

where $\dot{Q}$ is the heat release rate (kW), ρ_a is the air density (kg/m^3), c_p is the specific heat at constant pressure (kJ/(kg·K)), T_a is the ambient temperature (K), and g is the gravity acceleration (m/s^2).

The recommended D^*/δ_x should be 4∼16 [28]. Generally, a smaller grid size results in higher accuracy for numerical simulations; however, this also leads to longer simulation times. Grid quality verification was necessary to determine an appropriate grid size. The best grid size for $\dot{Q} = 3$ MW varies from 0.09 to 0.37 m, as determined by Eq. (1), and the recommended values of D^*/δ_x. Similarly, for $\dot{Q} = 5$ MW, the optimal grid size varies from 0.11 to 0.46 m, and for $\dot{Q} = 10$ MW, it varies from 0.15 to 0.6 m. Thus, this research picked the parameters $\dot{Q} = 5$ MW, $D_e = 60$ m, $V = 60$ m^3/s, $d_1 = d_2 = 30$ m for the sensitivity analysis of the gird by using three different mesh sizes (0.2, 0.25, 0.35 m) to verify the independence of the mesh under three HRRs. As depicted in Fig. 2, the longitudinal temperature distribution is similar for 0.2 m grid size and 0.25 m grid size. However, the deviation in the simulation results for the 0.3 m grid size is markedly apparent. In order to achieve a compromise between simulation time and accuracy, the 0.25 m grid size was selected.

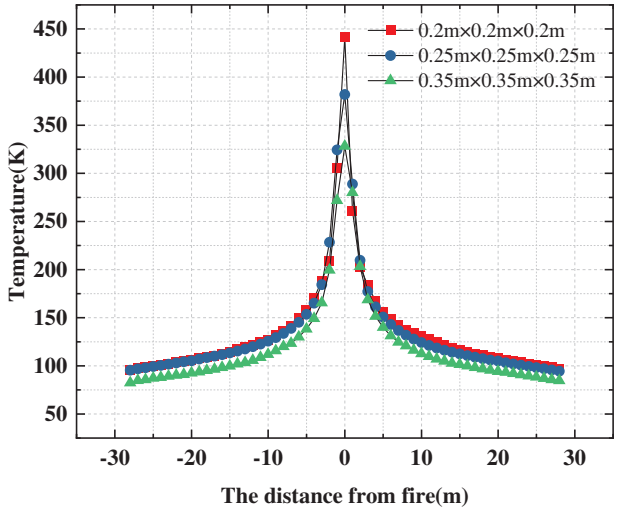

Figure 2: Variations in mesh diameters affect the temperature distribution along the length of the ceiling ($\dot{Q} = 5$ MW, $D_e = 60$ m, $V = 60$ m^3/s, $d = 30$ m)

3 Results and Discussion

3.1 Influence of Distance between Fire and Smoke Outlet on Mass Flow Rate

When smoke transitions from the point of origin to the ventilation outlet, a large volume of air is drawn in. This mostly happens during three stages: plume rise (Stage 1), one-dimensional longitudinal

spreading (Stage 2), and smoke discharge from the smoke outlet (Stage 3) [29], as represented in Fig. 3. This work specifically examines the phenomenon of air entrainment in Stage 3.

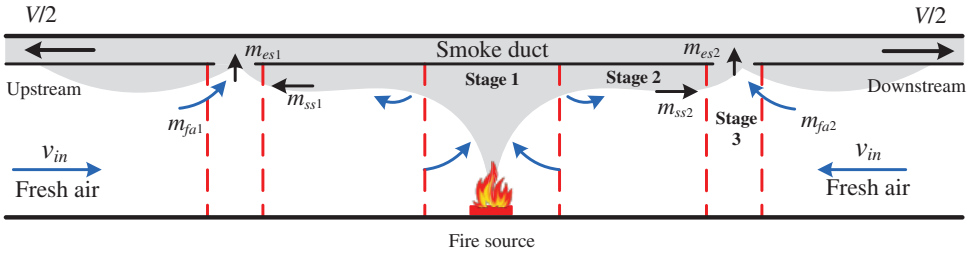

Figure 3: Illustration depicting the centralized smoke extraction system

The smoke mass flow rate emitted from the smoke outlet is determined by adding the smoke mass flow rate generated at the fire source to the fresh air mass flow rate that is drawn in, as indicated by the following equation:

$$\dot{m}_{es} = \dot{m}_{fa} + \dot{m}_{ss} \tag{2}$$

where $\dot{m}_{es}$ is the mass flow rate expelled from the exhaust (kg/s), $\dot{m}_{fa}$ is the fresh air mass flow rate (kg/s), $\dot{m}_{ss}$ is the smoke mass flow rate (kg/s).

Depending on the principle of energy conservation, the following equations could be expressed:

$$\dot{Q}_{es} = \dot{Q}_{ss} \tag{3}$$

$$\dot{Q}_{es} = c_p \dot{m}_{es} \Delta T_{es} = c_p \rho_s v_{es} S \Delta T_{es} \tag{4}$$

$$\dot{Q}_{ss} = c_p \dot{m}_{ss} \Delta T_{ss} \tag{5}$$

where $\dot{Q}_{es}$ is the heat expelled from the smoke outlet (kW), $\dot{Q}_{ss}$ represents the heat of smoke produced by the fire burning (kW), ΔT_{es} is the temperature increase at the smoke outlet (K), ΔT_{ss} is the temperature increase at the smoke outlet without centralized smoke exhaust (K), ρ_s is the smoke density at the smoke outlet (kg/m^3), v_{es} is the velocity at the smoke outlet (m/s), and S denotes the area of the smoke outlet (m^2).

Combining Eqs. (4) and (5) with Eq. (2), the following equation can be expressed:

$$\frac{\dot{m}_{fa}}{\dot{m}_{es}} = 1 - \frac{\Delta T_{es}}{\Delta T_{ss}} \tag{6}$$

The fresh air mass flow rate and smoke mass flow rate can be calculated using Eqs. (2) and (6). Fig. 4 demonstrates the trend of mass flow rate with longitudinal fire positions at the smoke outlet, considering various heat release rates. Fig. 4a demonstrates that $\dot{m}_{ss1}$ at the upstream smoke outlet exhibits a steady increase as d_1 grows, while $\dot{m}_{fa1}$ at the upstream smoke outlet experiences a gradual drop with the increase of d_1. Furthermore, $\dot{m}_{fa}$ is oppositely related to HRR, while $\dot{m}_{ss}$ is directly related to HRR, assuming the same positioning conditions. The closer the fire source is to the smoke outlet, the higher the temperature of the smoke below the smoke outlet. The greater the difference in density between the smoke and the ambient air, the greater the mass flow rate of air at the upstream smoke outlet. Thus, $\dot{m}_{fa1}$ increases as the density difference between the smoke and the ambient air becomes higher. Fig. 4b illustrates the variation in $\dot{m}_{fa2}$ and $\dot{m}_{ss2}$; both $\dot{m}_{fa2}$ and $\dot{m}_{ss2}$ exhibit minimal variations at the outlet when fire is at different positions. The distance between the fire and the downstream smoke

outlet is greater compared to the upstream outlet, resulting in a negligible impact on the temperature difference beneath the smoke outlet due to varying fire locations. Accordingly, the fresh air mass flow rate and the smoke mass flow rate at the exhaust vent downstream changed a little.

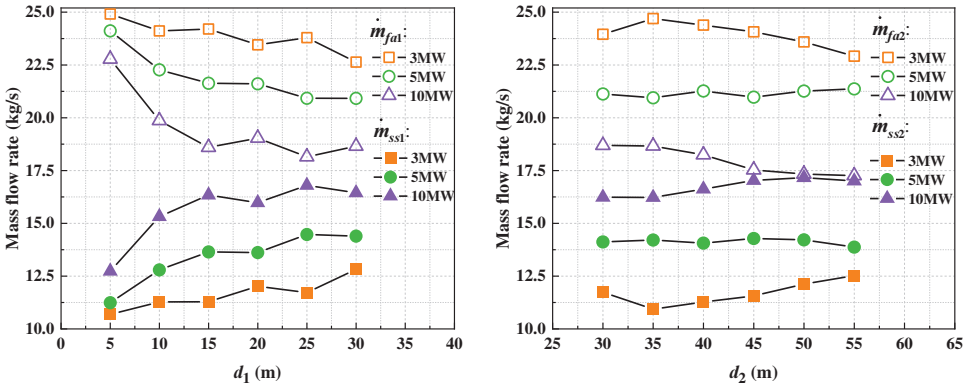

(a) (b)

Figure 4: Evolution of mass flow rate with different HRRs and different distances between fire and smoke outlet ($V = 60$ m^3/s, $D_e = 60$ m) for (a) $\dot{m}_{fa1}$ and $\dot{m}_{ss1}$ at the upstream smoke outlet; (b) $\dot{m}_{fa2}$ and $\dot{m}_{ss2}$ at the downstream smoke outlet

Fig. 5 displays the changes in the $\dot{m}_{fa}$ and $\dot{m}_{ss}$ as the exhaust volumetric flow rates and longitudinal fire positions vary. When the smoke exhaust volumetric flow rate is held constant, $\dot{m}_{fa1}$ falls as the distance d_1 increases, whereas $\dot{m}_{ss1}$ grows with d_1. When d_1 is constant, the fresh air and smoke mass flow rates both increase with V because of the enhanced extraction effect. From Fig. 5b, $\dot{m}_{fa2}$ and $\dot{m}_{ss2}$ are essentially unchanged with d_2. When V varies, there is a substantial increase in $\dot{m}_{fa2}$, but a small increase in $\dot{m}_{ss2}$.

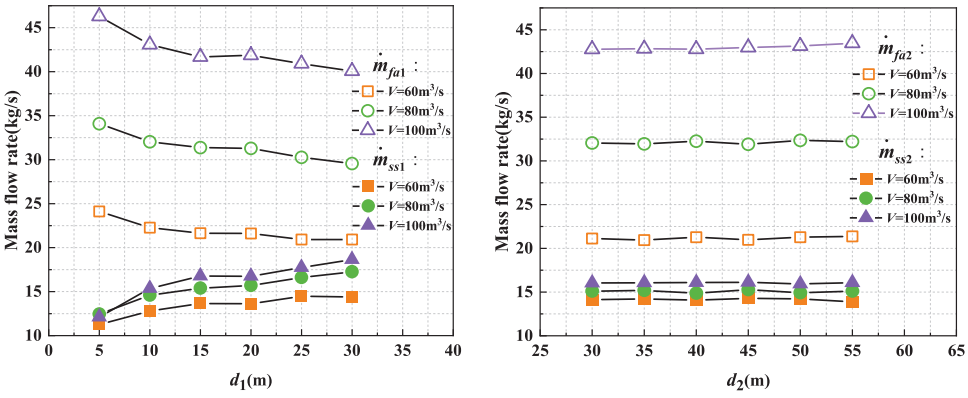

(a) (b)

Figure 5: Evolution of mass flow rate with different smoke extraction rates and different distances between fire and smoke outlet ($\dot{Q} = 5$ MW, $D_e = 60$ m) for (a) $\dot{m}_{fa1}$ and $\dot{m}_{ss1}$ at the upstream smoke outlet; (b) $\dot{m}_{fa2}$ and $\dot{m}_{ss2}$ at the downstream smoke outlet

Fig. 6 illustrates the changes in $\dot{m}_{fa}$ and $\dot{m}_{ss}$, influenced by varying intervals between two smoke outlets and different longitudinal fire positions. $\dot{m}_{fa1}$ falls in proportion to the ratio of d_1 to D_e, while

$\dot{m}_{ss1}$ increases in proportion to the same ratio, as depicted in Fig. 6a. However, $\dot{m}_{fa2}$ and $\dot{m}_{ss2}$ change with d_2/D_e insignificantly from Fig. 6b. The ratio d/D_e indicates the relative location of the fire origin between the smoke outlets. Hence, the alterations in the mass flow rate are affected negligibly by alterations in the intervals between smoke outlets.

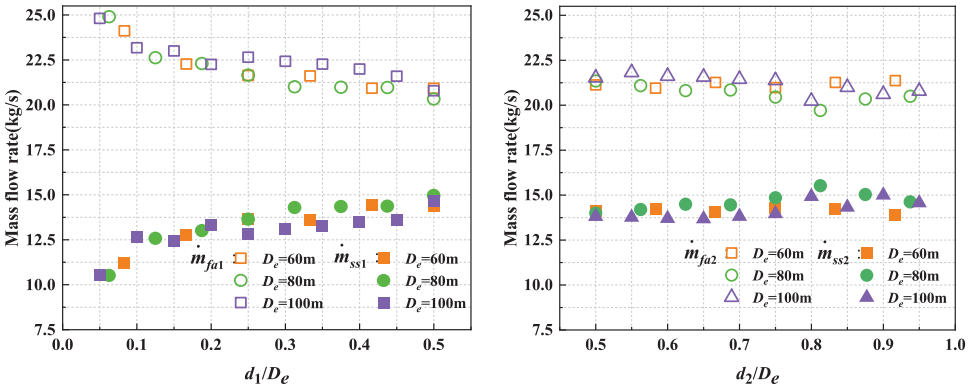

(a) (b)

Figure 6: Evolution of mass flow rate with different distances between two smoke outlets and different distances between fire and smoke outlet ($\dot{Q} = 5$ MW, $V = 60$ m^3/s) for (a) $\dot{m}_{fa1}$ and $\dot{m}_{ss1}$ at the upstream smoke outlet; (b) $\dot{m}_{fa2}$ and $\dot{m}_{ss2}$ at the downstream smoke outlet

3.2 Influence of the Distance between Fire and Smoke Outlet on Heat Exhaust Coefficient

Given the unpredictability of fire locations, the length from the fire to its nearest upstream and downstream smoke outlets can vary. Consequently, this impacts the heat transfer both before and after the fire source. Define the heat exhaust coefficient as the ratio of the heat expelled from the exhaust outlet to $\dot{Q}$, and it can be expressed by Eq. (7):

$$E = \frac{\dot{Q}_{es}}{\dot{Q}} = \sum E_i = \sum \frac{\dot{Q}_{es,i}}{\dot{Q}} \tag{7}$$

where E is the heat exhaust coefficient of the centralized smoke extraction system, E_i is the heat exhaust coefficient of a single smoke outlet, and $\dot{Q}_{es,i}$ is the heat released from a single exhaust outlet (kW).

When the fire source is equidistant from both sides of the smoke outlet, two outlets should discharge the same heat. In this scenario, a single smoke outlet's heat exhaust coefficient can be denoted as E_0, which is associated with $\dot{Q}$, V, D_e, H, ρ_a, T_a, c_p and g. As a result, E_0 can be expressed by Eq. (8):

$$E_0 = f\left(\dot{Q}, V, D_e, H, \rho_a, T_a, c_p, g\right) \tag{8}$$

The fundamental magnitudes are selected as the primary quantities, representing the four basic physical quantities ρ_a, c_p, T_a, and H. Eq. (9) can be obtained as follows:

$$\begin{cases} \pi_1 = \rho_a^{\alpha_1} c_p^{\beta_1} T_a^{\gamma_1} H^{\varepsilon_1} \dot{Q} = [ML^{-3}]^{\alpha_1} [L^2T^{-2}\theta^{-1}]^{\beta_1} \theta^{\gamma_1} L^{\varepsilon_1} [ML^2T^{-3}] \\ \pi_2 = \rho_a^{\alpha_2} c_p^{\beta_2} T_a^{\gamma_2} H^{\varepsilon_2} V = [ML^{-3}]^{\alpha_2} [L^2T^{-2}\theta^{-1}]^{\beta_2} \theta^{\gamma_2} L^{\varepsilon_2} [L^3T^{-1}] \\ \pi_3 = \rho_a^{\alpha_3} c_p^{\beta_3} T_a^{\gamma_3} H^{\varepsilon_3} D_e = [ML^{-3}]^{\alpha_3} [L^2T^{-2}\theta^{-1}]^{\beta_3} \theta^{\gamma_3} L^{\varepsilon_3} L \\ \pi_4 = \rho_a^{\alpha_4} c_p^{\beta_4} T_a^{\gamma_4} H^{\varepsilon_4} g = [ML^{-3}]^{\alpha_4} [L^2T^{-2}\theta^{-1}]^{\beta_4} \theta^{\gamma_4} L^{\varepsilon_4} [LT^{-2}] \end{cases} \tag{9}$$

In accordance with similarity theory, Eq. (9) should be substituted with the Eq. (10):

$$E_0 = f\left(\frac{\dot{Q}}{\rho_a c_p^{3/2} T_a^{3/2} H^2}, \frac{V}{c_p^{1/2} T_a^{1/2} H^2}, \frac{D_e}{H}, \frac{Hg}{c_p T_a}\right)$$
$$= f\left(\frac{\dot{Q}}{\rho_a c_p T_a g^{1/2} H^{5/2}}, \frac{V}{H^{5/2} g^{1/2}}, \frac{D_e}{H}\right)$$
$$= f\left(\dot{Q}^*, V^*, D_e^*\right) \tag{10}$$

From Eq. (10), E_0 is related to $\dot{Q}^*$, V^*, and D_e^*. Fig. 7a illustrates the influence of varying HRRs on E_0, demonstrating a decrease as the $\dot{Q}^*$ increases for a constant exhaust volumetric flow rate. This phenomenon occurs because there is a direct connection between the increase in heat release rate and the corresponding increase in the production of smoke mass flow rate. Moreover, the mass flow rate of expelled smoke remains constant, resulting in a decrease in the heat exhaust coefficient. Fig. 7b depicts the relationship between different exhaust volumetric flow rates and E_0. It shows that once the V^* increases, E_0 also increases. More smoke is exhausted and, subsequently, an elevation in the heat exhaust coefficient. Fig. 7c depicts the impact of various smoke outlet intervals on the heat exhaust coefficient E_0; notably, E_0 decreases as the dimensionless smoke outlet spacing increases. This phenomenon occurs because an increase in smoke outlet spacing lengthens the distance smoke travels within the tunnel. As a result, this lengthening increases the heat transfer between the tunnel walls and hot smoke, reducing the amount of heat that is released from the smoke outlets. The decrease in heat discharge leads to a fall in the heat exhaust coefficient.

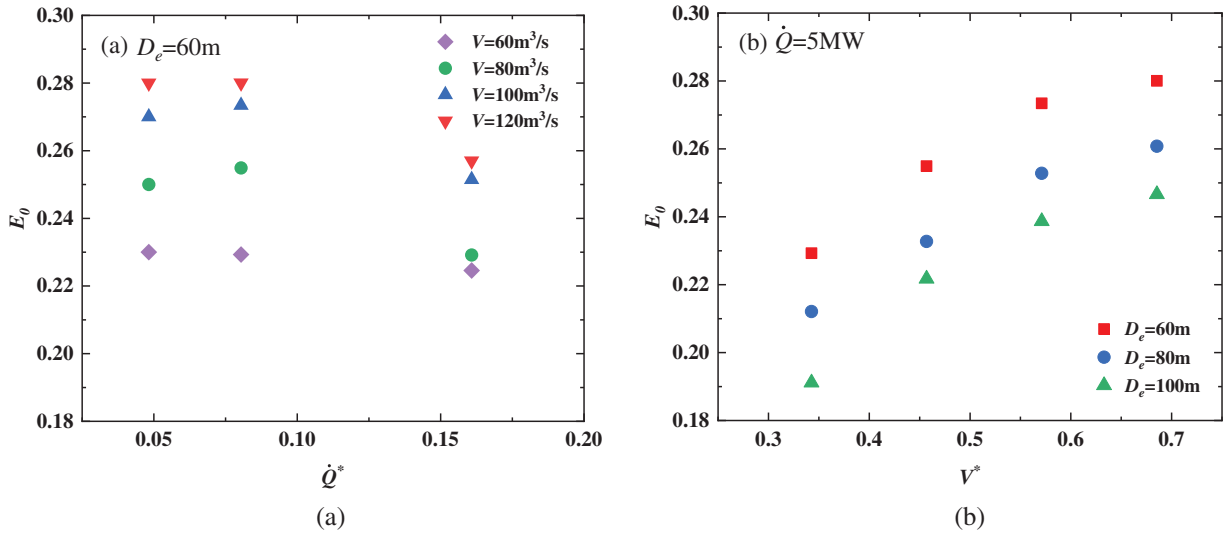

Figure 7: (Continued)

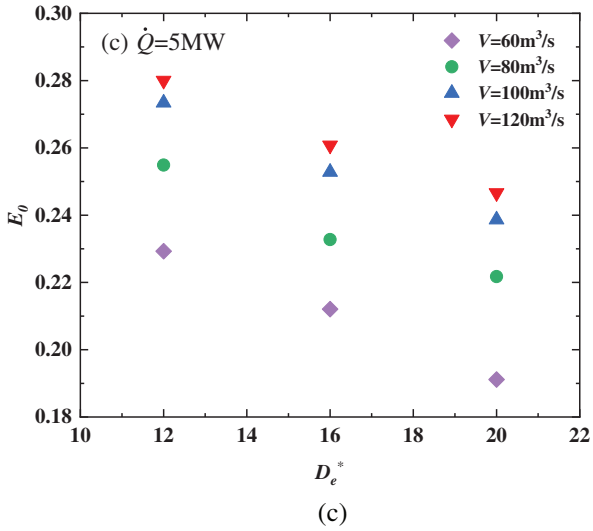

Figure 7: Evolution of E_0 (a) with different heat release rates, (b) with different smoke extraction rates, (c) with different distances between two smoke outlets

To explore the relationship among E_0, $\dot{Q}^*$, V^*, and D_e^*, The Eq. (11) provided expresses the heat exhaust coefficient E_0.

$$E_0 = \chi V^{*\lambda} D_e^{*\tau} \dot{Q}^{*\sigma} \tag{11}$$

where χ, λ, τ, σ are the coefficients.

By analyzing the data we obtained the formula for E_0 as shown in Eq. (12). As illustrated in Fig. 8, there is a good correlation between the heat exhaust coefficient E_0 and the predicted values for different heat release rates, smoke extraction volumetric rates, and the spacing of smoke outlets. Its correlation coefficient is 0.95, indicating the reliability of the predictive model.

$$E_0 = 0.57 \frac{V^{*0.3}}{D_e^{*0.3} \dot{Q}^{*0.06}} \tag{12}$$

Fig. 9 depicts the variation in E_i for a single smoke exhaust outlet as the longitudinal location of the fire source is altered. There is a noticeable pattern showing that E_i decreases as the length from the fire source to the smoke outlet rises. This phenomenon occurs because there is increased heat transmission between the tunnel walls and hot smoke. As a result, less heat is released from the smoke outlet, leading to a decrease in E_i. Therefore d has an impact on the heat transfer occurring at the smoke outlets. Furthermore, the tunnel heat exhaust coefficient is influenced by d_1 and d_2.

The previous investigation indicates a negative link between E_i and the distance separating the fire source from the smoke exhaust outlet. Therefore, it is implied that the correlation between E_i/E_0 and d/D_e can be mathematically represented by the subsequent equation:

$$\frac{E_i}{E_0} = f\left(\frac{d}{D_e}\right) \tag{13}$$

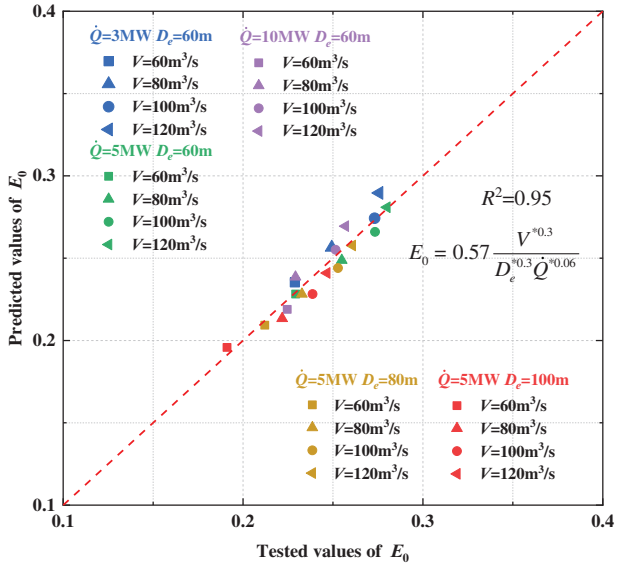

Figure 8: Test results *vs*. results by the proposed model

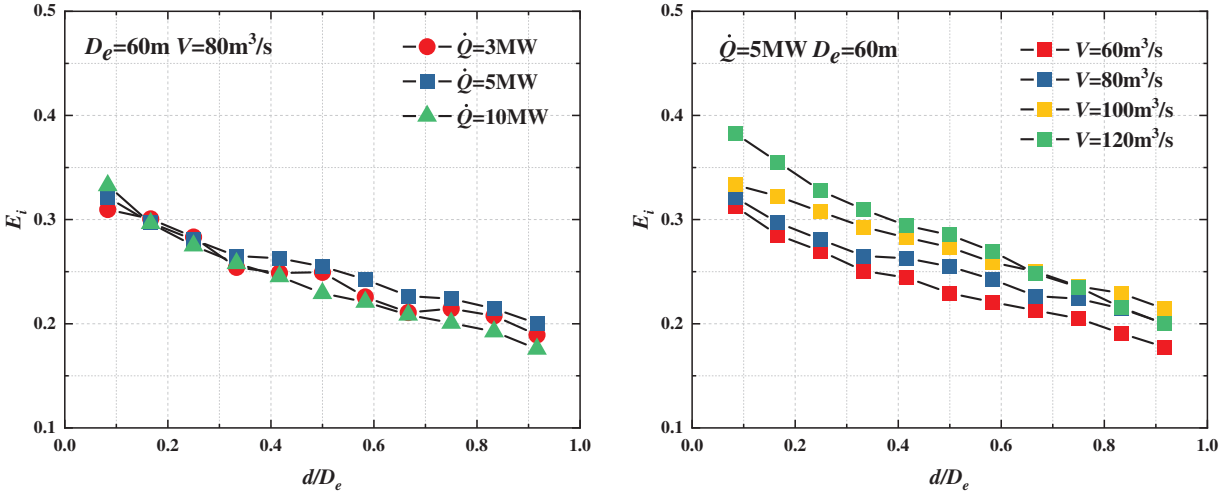

Figure 9: (Continued)

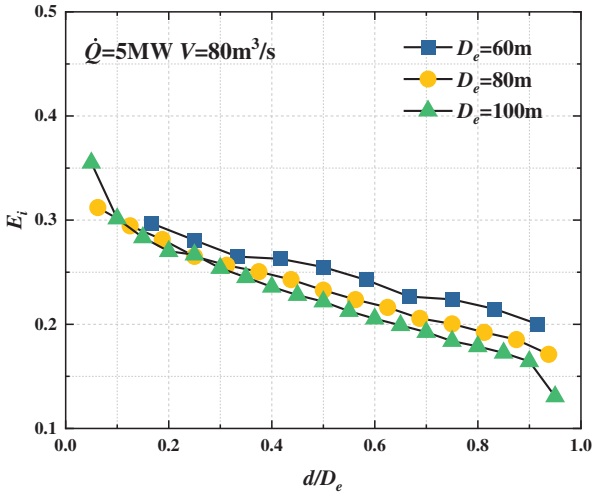

(c)

Figure 9: Evolution of E_i with different distances between the fire and the smoke outlet for (a) D_e = 60 m, V = 80 m^3/s; (b) $\dot{Q}$ = 5 MW, D_e = 60 m; (c) $\dot{Q}$ = 5 MW, V = 80 m^3/s

Fig. 10 demonstrates the functional relationship between E_i/E_0 and d/D_e. It can be seen easily that there is a linear function between E_i/E_0 and d/D_e. The constant term and slope of this function can be derived through fitting with data. It can be observed that for varying smoke outlet intervals, the slope (k_1) of the fitted functional relationship decreases as the spacing of smoke outlets increases, according to Fig. 10b,d,e. Since the functional equation passes the point (0.5, 1), the slope can express the intercept of the equation. To unify the functional expression under different smoke outlet intervals, the relationship between smoke outlet intervals and k_1 can be represented by the following formula:

$$k_1 = -\frac{1}{200}D_e - 0.3 \tag{14}$$

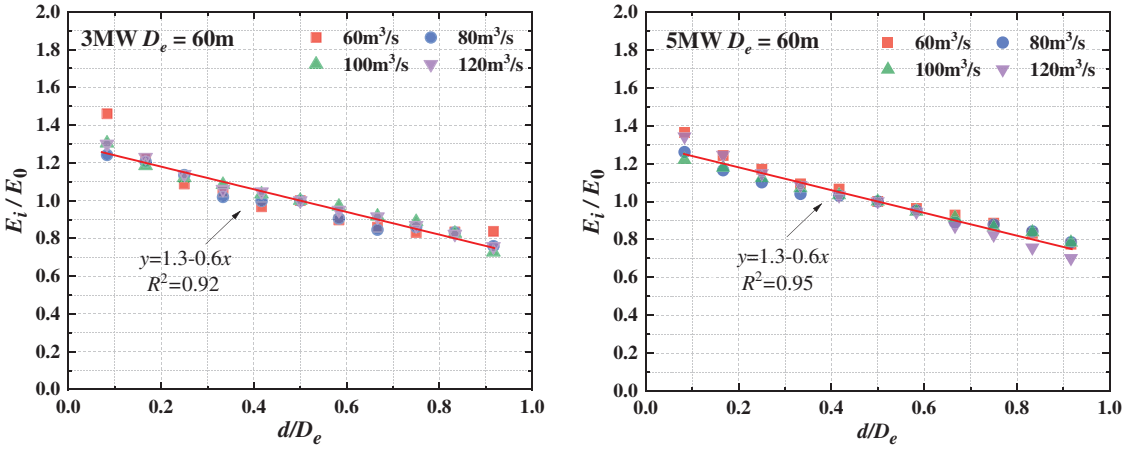

(a) (b)

Figure 10: (Continued)

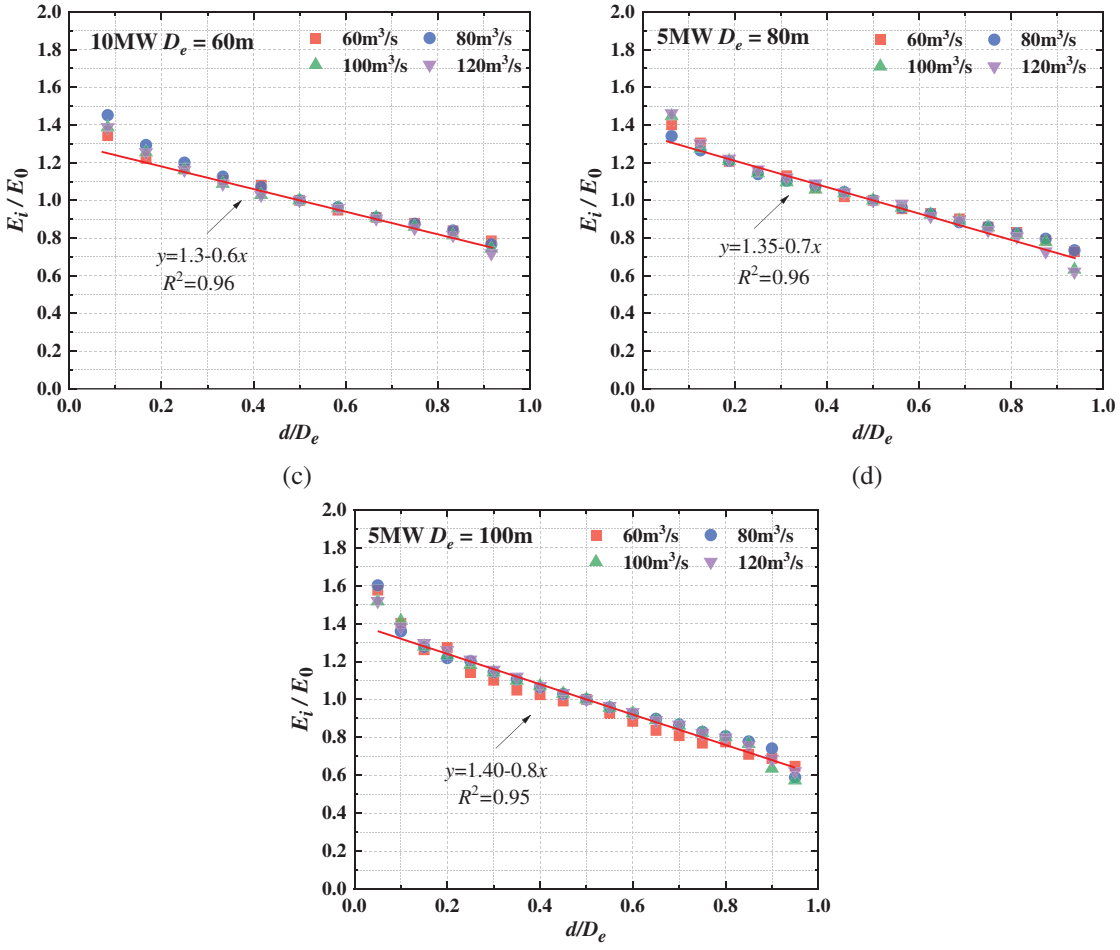

Figure 10: The relationship between E_i/E_0 and d/D_e for (a) $\dot{Q} = 3$ MW, $D_e = 60$ m; (b) $\dot{Q} = 5$ MW, $D_e = 60$ m; (c) $\dot{Q} = 10$ MW, $D_e = 60$ m; (d) $\dot{Q} = 5$ MW, $D_e = 80$ m; (e) $\dot{Q} = 5$ MW, $D_e = 100$ m

Bringing Eq. (14) into the relationship obtained from the fit, the following equation can be derived:

$$\frac{E_i}{E_0} = 1.15 + \frac{1}{400}D_e - \left(\frac{D_e}{200} + 0.3\right)\frac{d}{D_e} \tag{15}$$

By linking Eqs. (12) and (15), we can derive a prediction model Eq. (16) for the E_i, as displayed in Fig. 11. The calculated heat exhaust coefficient closely corresponds to the expected values, indicating a clear alignment between the two parameters. Hence, the prediction model can more effectively describe the heat exhaust coefficients associated with various longitudinal fire source locations within the tunnel.

$$E_i = 0.57\frac{V^{*0.3}}{D_e^{*0.3}Q^{*0.06}}\left[1.15 + \frac{1}{400}D_e - \left(\frac{D_e}{200} + 0.3\right)\frac{d}{D_e}\right] \tag{16}$$

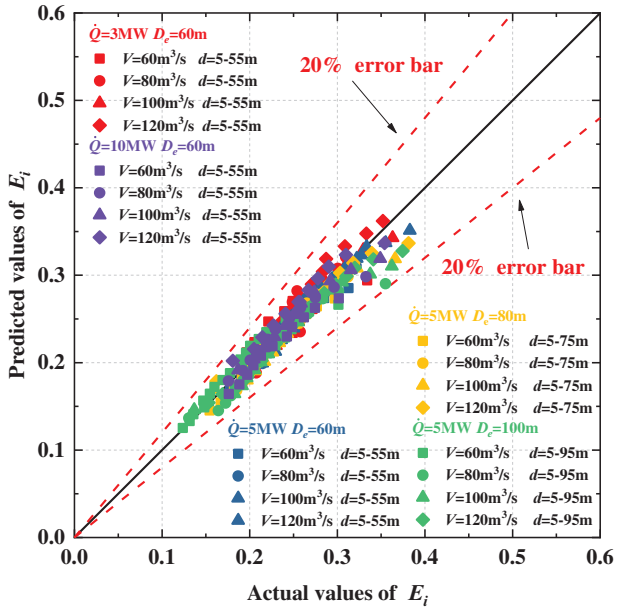

Figure 11: Test results *vs*. results by the proposed model

3.3 Influence of the Distance between Fire and Smoke Outlet on Smoke Spreading Distance

The length from the smoke exhaust outlet to the smoke front was defined as L_b which is called smoke spreading distance [30]. Fig. 12 illustrates the smoke movement under various fire source positions. The figure clearly demonstrates that while $\dot{Q} = 5$ MW, $V = 80$ m^3/s, the distance at which the smoke spreads upstream decreases with d_1 increases. Conversely, the downstream smoke spreading distance increases inversely with the decreased d_2. When the distance between the fire source and the smoke outlet is shorter, the smoke is pulled more forcefully towards the outlet, resulting in an increased upstream movement of the smoke. Consequently, the distance that smoke spreads in the upstream direction is greater than the distance it spreads in the downstream direction.

Li et al. [13] gave a model for calculating the dimensionless smoke spreading distance combined with theoretical analysis, which can be represented by the subsequent equation:

$$\frac{L_b}{H} = \begin{cases} 18.5\ln\left(0.81\dot{Q}^{*1/3}/v^*\right), & \dot{Q}^* \le 0.15 \\ 18.5\ln\left(0.43/v^*\right), & \dot{Q}^* > 0.15 \end{cases} \tag{17}$$

$$\dot{Q}^* = \frac{\dot{Q}}{\rho_a c_p T_a g^{1/2} H^{5/2}} \tag{18}$$

$$v^* = \frac{v}{\sqrt{gH}} \tag{19}$$

where v is the longitudinal velocity, m/s; v^* is the dimensionless longitudinal velocity, m/s.

When $d_1 = d_2$, the heat produced by the fire source is discharged through the smoke outlets. Simultaneously, the remaining heat carried by the one-sided smoke in the tunnel due to the extraction effect $\dot{Q}_e^*$ could be written as:

$$\dot{Q}_e^* = \frac{1}{2}\dot{Q} - c_p\dot{m}_{es}\Delta T_{es} = \frac{1}{2}\dot{Q} - c_p\rho_s v_{es} S\Delta T_{es} \tag{20}$$

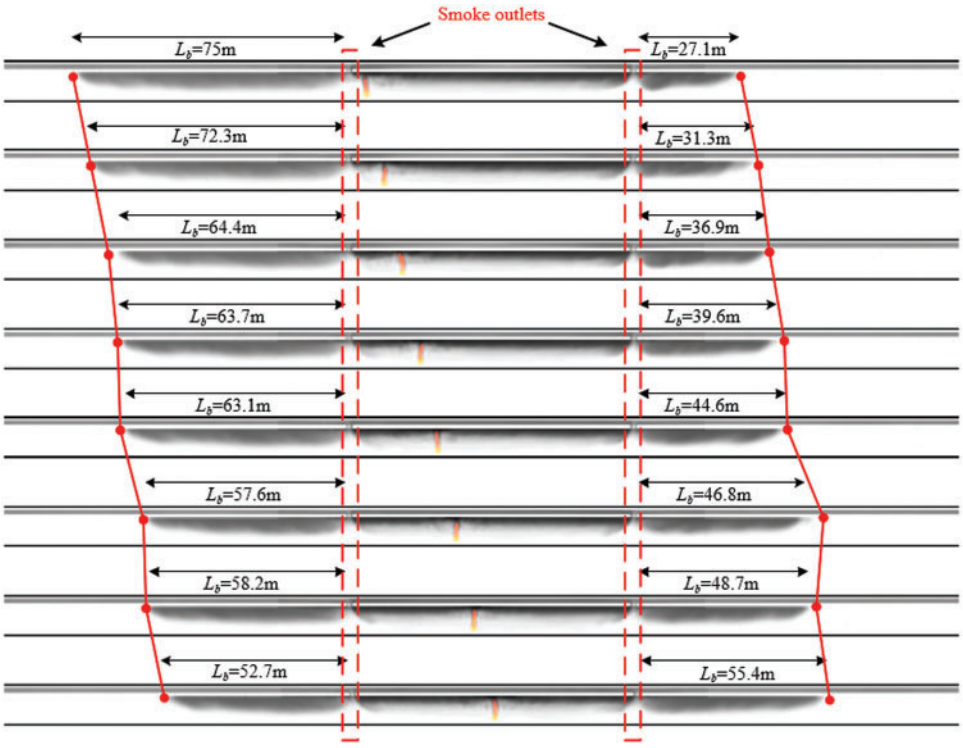

Figure 12: Evolution of smoke spread distance with varying longitudinal fire locations ($\dot{Q} = 5$ MW, $D_e = 80$ m, $V = 80$ m^3/s)

The dimensionless induced flow velocity can be defined as:

$$v_{in}^{*} = \frac{\dot{m}_{es}/2A\rho_a}{\sqrt{gH}} \tag{21}$$

where A is the area of the tunnel cross-section, m^2; v_{in}^{*}: is the dimensionless velocity of the induced air flow, m/s.

According to Eqs. (17), (20) and (21), in the scenario where the fire source exists at the midpoint of the tunnel, there would be a balance between the spread distance upstream and downstream. Therefore, only one side of the smoke spreading distance is considered, as displayed in Fig. 13. According to Fig. 13, the formulation can provide a more precise description of the smoke spreading distance with different HRRs, exhaust volumetric flow rates, and smoke outlet intervals. Since $\dot{Q}_e^{*}$ is less than 0.15 in this investigation, the model for prediction for the dimensionless spreading distance of smoke ($L_{b,mid}$) in the situation where the fire source is at the midpoint of the tunnel could be written as follows:

$$\frac{L_{b,mid}}{H} = 24.8 \ln\left(0.81\dot{Q}_e^{*1/3}/v_{in}^{*}\right) \tag{22}$$

The dimensionless quantity $d^{*} = d/H$ is introduced. As depicted in Fig. 14, the change rate of the smoke spreading distance with d^{*} varies depending on $\dot{Q}$ and V. The change rate of the smoke spreading distance with d^{*} is basically the same under different interval conditions.

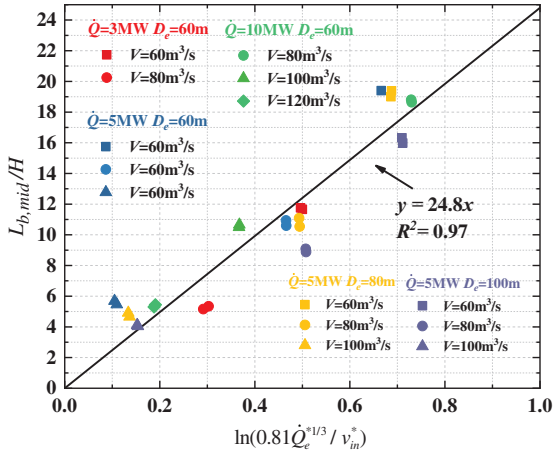

Figure 13: The relationship between $L_{b,mid}/H$ and $\ln\left(0.81\dot{Q}_e^{*1/3}/v_{in}^*\right)$

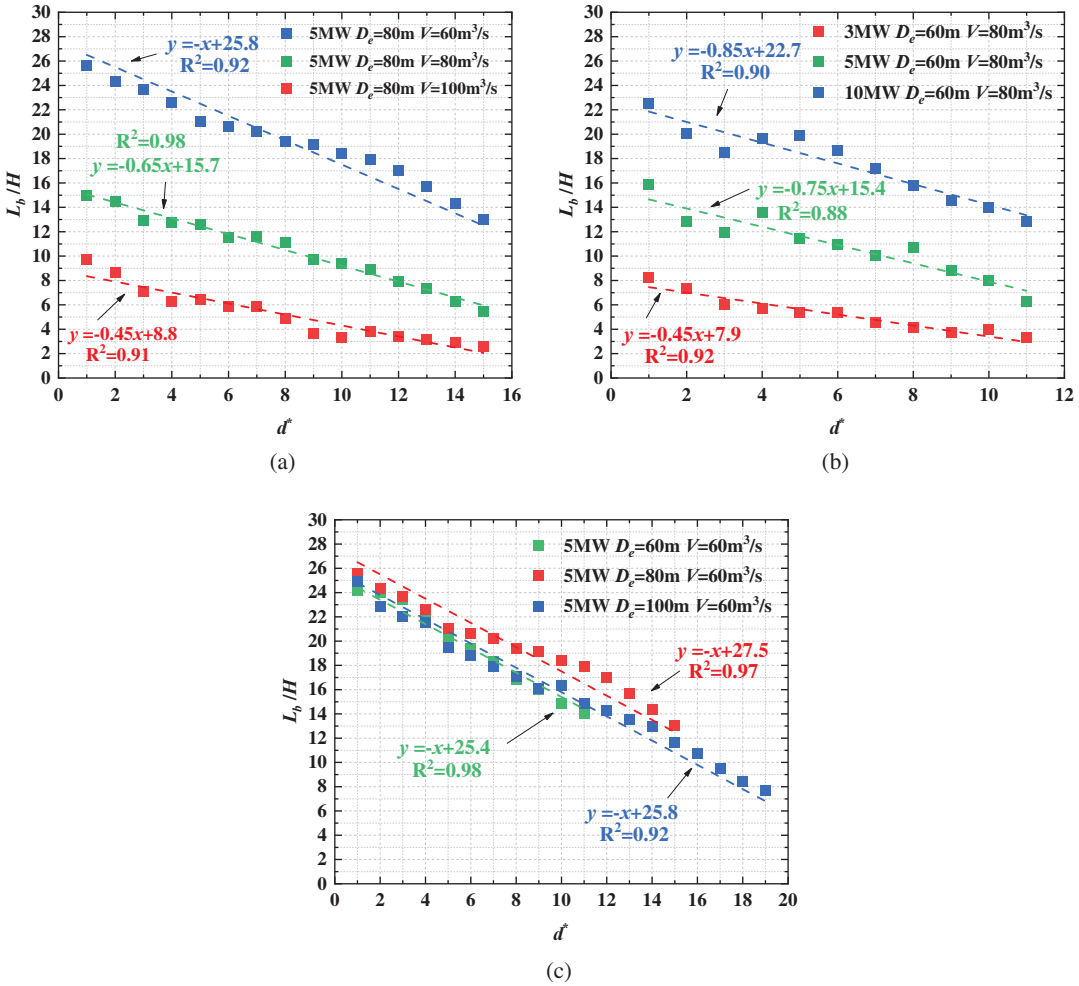

Figure 14: The relation between the smoke spreading distance and d^*: (a) the effect of smoke extraction volumetric rates; (b) the effect of heat release rates; (c) the effect of smoke outlets spacing

Therefore, it is assumed that the relationship among the rate of change (k_2), d^*, V^*, can be given by Eq. (23):

$$k_2 = \eta \dot{Q}^{*\varphi} V^{*\zeta} \tag{23}$$

where η, φ, ζ are the coefficients.

As shown in Fig. 15, to determine the relationship among k_2, $\dot{Q}^*$, and V^*, all simulated conditions were fitted with dimensionless $\dot{Q}^*$ and dimensionless V^* to obtain an empirical equation for k_2:

$$k_2 = -0.7\left(\frac{\dot{Q}^*}{V^{*3}}\right)^{0.5} \tag{24}$$

The smoke spreading distance at other fire locations can be expressed by Eq. (25):

$$\frac{L_b}{H} = \frac{L_{b,mid}}{H} + k_2\,(d^* - d_0) \tag{25}$$

$$d_0 = \frac{D_e}{2}/H \tag{26}$$

where d_0 is the dimensionless parameter when the fire source is at the midpoint of two smoke outlets.

Therefore, by combining Eqs. (22), (24) and (25), a model for predicting the smoke spreading distance at different locations can be obtained:

$$\frac{L_b}{H} = 24.8 \ln\left(0.81 Q_e^{*1/3}/v_{in}^*\right) - 0.7\left(\frac{\dot{Q}^*}{V^{*3}}\right)^{0.5}\left(\frac{D_e}{2H} - d^*\right) \tag{27}$$

All the test results were compared to the predictions, as shown in Fig. 16. The prediction model can better predict the dimensionless smoke spreading distance with different HRRs, different intervals of smoke outlets, and different exhaust volumetric flow rates.

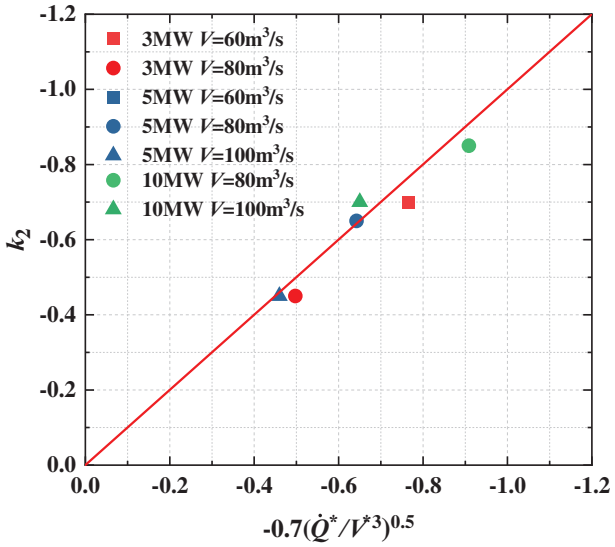

Figure 15: The relationship between k_2 and $-0.7\left(\dot{Q}^*/V^{*3}\right)^{0.5}$

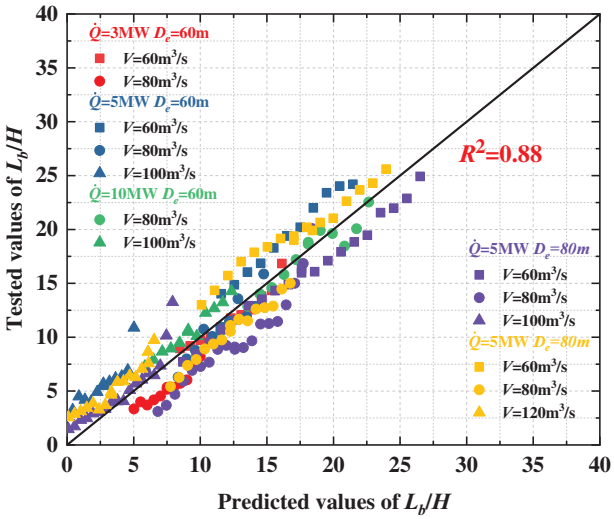

Figure 16: Test results *vs*. results by the proposed model

4 Conclusions

This paper examined the alteration in smoke flow characteristics resulting from the relative longitudinal position of tunnel-centralized smoke exhaust outlets and the fire source. This study encompassed four variables: heat release rates, exhaust volumetric flow rates, longitudinal fire locations, and intervals between smoke outlets. The main findings can be summarized as follows:

(1) The fresh air mass flow rate at the smoke outlet is directly proportional to smoke extraction volumetric rate and inversely proportional to heat release rate. The variation of the smoke mass flow rate is opposite to the fresh air mass flow rate. The spacing of smoke outlets has little effect on both air mass flow rate and smoke mass flow rate.

(2) A predictive model for heat exhaust coefficient was derived. The heat exhaust coefficient increases with the smoke extraction volumetric rate and decreases with the increasing distance between the fire source and the smoke outlet and heat release rate.

(3) The smoke spreading distance diminishes with the increased distance between the fire source and the smoke outlet. A model was obtained to predict the smoke spreading distance by considering various heat release rates, smoke extraction volumetric rates, and the spacing of smoke outlets.

The results of this study can contribute to technical methods for tunnel smoke emission prevention and control. However, the study does not consider the effect of the diameter of smoke outlets, the area of the tunnel section and the longitudinal ventilation. The smoke flow characteristics under the relative longitudinal positions of tunnel-centralized smoke outlets and the fire source will be studied in the future by taking these factors into account.

Acknowledgement: The authors acknowledge the support of Central South University's High-Performance Computing Center.

Funding Statement: The authors received no specific funding for this study.

Author Contributions: The authors confirm contribution to the paper as follows: study conception and design: Liang Yi; data collection and analysis: Zhiqiang Lei; interpretation of results: Yaolong Yin, Zhisheng Xu; draft manuscript preparation: Zhiqiang Lei, Houlin Ying. All authors reviewed the results and approved the final version of the manuscript.

Availability of Data and Materials: There is no data that is unavailable in this study.

Conflicts of Interest: The authors declare they have no conflicts of interest to report regarding the present study.

References

1. Heidarinejad G, Mapar M, Pasdarshahri H. A comprehensive study of two fire sources in a road tunnel: considering different arrangement of obstacles. Tunnelling Undergr Space Technol. 2016 Oct 1;59:91–9. doi:10.1016/j.tust.2016.06.016.
2. Shaw T, Gibson T, Karlovšek J, Emberley R, Torero JL. Experimental evaluation of the heat flux induced by tunnel fires. Tunnelling Undergr Space Technol. 2016 Nov 1;60:49–55. doi:10.1016/j.tust.2016.07.015.
3. Carvel RO, Beard AN, Jowitt PW. Fire spread between vehicles in tunnels: effects of tunnel size, longitudinal ventilation and vehicle spacing. Fire Technol. 2005 Oct;41(4):271–304. doi:10.1007/s10694-005-4050-y.
4. Carvel R. A review of tunnel fire research from edinburgh. Fire Saf J. 2019 Apr;105:300–6. doi:10.1016/j.firesaf.2016.02.004.
5. Alarie Y. Toxicity of fire smoke. Crit Rev Toxicol. 2002;32(4):259–89. doi:10.1080/20024091064246.
6. Vauquelin O. Experimental simulations of fire-induced smoke control in tunnels using an "air-helium reduced scale model": principle, limitations, results and future. Tunnelling Undergr Space Technol. 2008 Mar 1;23(2):171–8. doi:10.1016/j.tust.2007.04.003.
7. Li L, Gao Z, Ji J, Han J, Sun J. Research on the phenomenon of plug-holing under mechanical smoke exhaust in tunnel fire. Procedia Eng. 2013;62:1112–20. doi:10.1016/j.proeng.2013.08.168.
8. Jiang X, Liu M, Wang J, Li K. Study on air entrainment coefficient of one-dimensional horizontal movement stage of tunnel fire smoke in top central exhaust. Tunnelling Undergr Space Technol. 2016;60: 1–9. doi:10.1016/j.tust.2016.07.010.
9. Zhao P, Yuan Z, Yu N, Liang C. Effect of heat release rate and exhaust vent settings on the occurrence of plug-holing during tunnel fires with two-point extraction ventilation. Tunnelling Undergr Space Technol. 2020 Dec;106:103617. doi:10.1016/j.tust.2020.103617.
10. Yi L, Wei R, Peng J, Ni T, Xu Z, Wu D. Experimental study on heat exhaust coefficient of transversal smoke extraction system in tunnel under fire. Tunnelling Undergr Space Technol. 2015 Jun;49:268–78. doi:10.1016/j.tust.2015.05.002.
11. Yan Z, Zhang Y, Guo Q, Zhu H, Shen Y, Guo Q. Numerical study on the smoke control using point extraction strategy in a large cross-section tunnel in fire. Tunnelling Undergr Space Technol. 2018 Dec 1;82:455–67. doi:10.1016/j.tust.2018.08.019.
12. Liu Y, Yang D. Experimental study on synergistic effect of exhaust vent layout and exhaust rate on performance of ceiling central smoke extraction in road tunnel fires. Int J Therm Sci. 2023 Jan;183:107886. doi:10.1016/j.ijthermalsci.2022.107886.
13. Li YZ, Lei B, Ingason H. Study of critical velocity and backlayering length in longitudinally ventilated tunnel fires. Fire Saf J. 2010 Nov 1;45(6):361–70.
14. Chen LF, Hu LH, Tang W, Yi L. Studies on buoyancy driven two-directional smoke flow layering length with combination of point extraction and longitudinal ventilation in tunnel fires. Fire Saf J. 2013 Jul 1;59: 94–101. doi:10.1016/j.firesaf.2013.04.003.

15. Chen LF, Hu LH, Zhang XL, Zhang XZ, Zhang XC, Yang LZ. Thermal buoyant smoke back-layering flow length in a longitudinal ventilated tunnel with ceiling extraction at difference distance from heat source. Appl Therm Eng. 2015 Mar;78:129–35. doi:10.1016/j.applthermaleng.2014.12.034.
16. Tang F, Li LJ, Mei FZ, Dong MS. Thermal smoke back-layering flow length with ceiling extraction at upstream side of fire source in a longitudinal ventilated tunnel. Appl Therm Eng. 2016 Aug;106(1–2):125–30. doi:10.1016/j.applthermaleng.2016.05.173.
17. Wang J, Yuan J, Fang Z, Tang Z, Qian P, Ye J. A model for predicting smoke back-layering length in tunnel fires with the combination of longitudinal ventilation and point extraction ventilation in the roof. Tunnelling Undergr Space Technol. 2018 Oct;80(4):16–25. doi:10.1016/j.tust.2018.05.022.
18. Jiang X, Liu M, Wang J, Li Y. Study on induced airflow velocity of point smoke extraction in road tunnel fires. Tunnelling Undergr Space Technol. 2018 Jan;71(1):637–43. doi:10.1016/j.tust.2017.09.020.
19. Liu Y, Yang D, Guo X. Theoretical model for predicting smoke back-layering length downstream of centralised ceiling exhaust vent in tunnel fires. Tunnelling Undergr Space Technol. 2023 Jul;137(4):105134. doi:10.1016/j.tust.2023.105134.
20. Ji J, Tan T, Gao Z, Wan H, Zhu J, Ding L. Numerical investigation on the influence of length-width ratio of fire source on the smoke movement and temperature distribution in tunnel fires. Fire Technol. 2019 May;55(3):963–79. doi:10.1007/s10694-018-00814-4.
21. Yu L, Wan H, Ji J. Asymmetric flow effect in a horizontal natural ventilated tunnel with different aspect ratios under the influence of longitudinal fire locations. Build Simul. 2021 Aug;14(4):1311–23. doi:10.1007/s12273-020-0742-y.
22. Yao Y, Li YZ, Ingason H, Cheng X. Numerical study on overall smoke control using naturally ventilated shafts during fires in a road tunnel. Int J Therm Sci. 2019 Jun;140:491–504. doi:10.1016/j.ijthermalsci.2019.03.016.
23. Tan T, Yu L, Ding L, Gao Z, Ji J. Numerical investigation on the effect of ambient pressure on mechanical smoke extraction efficiency in tunnel fires. Fire Saf J. 2021 Mar 1;120(3):103136. doi:10.1016/j.firesaf.2020.103136.
24. Mahmud HM, Moinuddin K. The effects of variation in shape of smoke reservoirs and numbers and distribution of smoke extraction points on the tenability within a compartment. Front Heat Mass Transfer. 2023;20:1–17. doi:10.5098/hmt.20.2.
25. Lafdal B, Djebbar R, Boulet P, Mehaddi R, Koutaiba E, Beji T, et al. Numerical study of the combustion regimes in naturally-vented compartment fires. Fire Saf J. 2022 Jul 1;131(2):103604. doi:10.1016/j.firesaf.2022.103604.
26. Lou Z, Huang J, Wang M, Zhang Y, Lv K, Yao H. Inhibition performances of lithium-ion battery pack fires by fine water mist in an energy-storage cabin: a simulation study. Phys Fluids. 2024 Apr 22;36(4):045141. doi:10.1063/5.0206160.
27. Li YZ, Ingason H. Overview of research on fire safety in underground road and railway tunnels. Tunnelling Undergr Space Technol. 2018 Nov;81:568–89. doi:10.1016/j.tust.2018.08.013.
28. McGrattan K, Hostikka S, Floyd J, McDermott R, Vanella M, Mueller E. Fire dynamics simulator (version 6): user's guide. Gaithersburg: National Institute of Standards and Technology; 2023.
29. Liu Q, Xu Z, Zhu J, Tagne SMS, Mahmood S, Xie B. Study of the impact of the distance between the lateral exhaust vent and ceiling on heat exhaust coefficient and air entrainment in tunnel fires. Tunnelling Undergr Space Technol. 2024 Jun 1;148:105766. doi:10.1016/j.tust.2024.105766.
30. Ingason H, Ying Zhen Li. Model scale tunnel fire tests with point extraction ventilation. J Fire Protect Eng. 2011 Feb 1;21(1):5–36. doi:10.1177/1042391510394242.